Electrical conductivity and resonant states of doped graphene considering next-nearest neighbor interaction

J.E. Barrios-Vargas [a] & Gerardo G. Naumis [a]

[a] Departamento de Física-Química, Instituto de Física, Universidad Nacional Autónoma de México (UNAM), Apartado Postal 20-364, México D.F. 01000, México

Available online: 08 Jul 2011

∩First

PLEASE SCROLL DOWN FOR ARTICLE

Electrical conductivity and resonant states of doped graphene considering next-nearest neighbor interaction

J.E. Barrios-Vargas and Gerardo G. Naumis*

Departamento de Física-Química, Instituto de Física, Universidad Nacional Autónoma de México (UNAM), Apartado Postal 20-364, México D.F. 01000, México

The next-nearest neighbor interaction (NNN) is included in a tight-binding Kubo formula calculation of the electronic spectrum and conductivity of doped graphene. As a result, we observe a wide variation of the behavior of the conductivity, as happens in carbon nanotubes, since the Fermi energy and the resonance peak are not shifted by the same amount when the NNN interaction is included. This finding may have a profound effect on the idea of explaining the minimal conductivity of graphene as a consequence of impurities or defects. Finally, we also estimate the mean free path and relaxation time due to resonant impurity scattering.

Keywords: graphene; disorder in graphene; electrical conductivity in graphene; electronic conduction; electronic density of states; electronic transport; mobility; tight-binding Hamiltonians; carbon nanostructures; carbon thin films; carbon-based materials

1. Introduction

Graphene has attracted a lot of interest since its experimental discovery in 2004 [1]. The interest in this carbon allotrope [2] is partly due to its room-temperature transport properties [3], as for example the high electronic mobility [4] and thermal conductivity [5], profiling nano-devices based on graphene [6]. From the theoretical viewpoint, charge carriers are described by massless Dirac fermions [4,7] as a consequence of the crystal symmetry. However, in the construction of electronic nano-devices, the use of pure graphene presents difficulties. For example, the conductivity is difficult to manipulate by means of an external gate voltage, which is a desirable feature required to build a FET transistor. This performance is related to the Klein paradox in relativistic quantum mechanics [7], or from a more standard outlook, as a consequence of the zero band gap. There are many proposals to solve this problem; for instance, by using quantum dots [8], a graphene nanomesh [9], an external electromagnetic radiation source [10,11] or by doping using impurities [12]. In fact, in a previous paper we showed that impurities lead to a metal–insulator transition since a mobility edge appears near the Fermi energy [12]. This prediction

---

*Corresponding author. Email: naumis@fisica.unam.mx

has been confirmed in doped graphene with H [13], which opens the possibility to build graphene-based narrow gap semiconductors [12]. Other groups have shown that graphene exhibits n-type semiconductor behavior when doped with N, Bi or Sb atoms; and p-type semiconductor behavior using B or Au atoms [14,15]. Still, there is much debate regarding the nature of the mobility transition, since in two-dimensional (2D) scaling theory, it is predicted that all states are localized in the presence of a finite amount of disorder [16,17].

The appearance of a mobility edge has its origins in the presence of resonant states when low impurity concentrations are considered [12]. Both type of states, localized and resonant, have an enhanced amplitude in the neighborhood of the impurity. Nevertheless, resonant states only trap electrons during a short time. Using a nearest neighbor (NN) tight-binding model, resonant states have been reported near the Fermi energy [18]. Furthermore, an approximate analytical expression was found for the resonant energy as a function of the impurity energy using the Lifshitz equation [19,20]. Pereira et al. [18] also noted that there is a slight difference between the resonance energy obtained from the Lifshitz equation, and the actual localization of the sharp resonance in the density of states (DOS) when the impurity energy is not so strong [18]. It is necessary to remark that only impurities with a self-energy greater than the band width are able to produce resonant states [21]. The presence of next-nearest neighbor interaction (NNN) shifts the Fermi energy and breaks the electron–hole symmetry [22]. Including NNN interaction, the DOS displays a sharp peak when a vacancy is considered like an impurity in the lattice [23]. Moreover, this peak is smeared by the NNN.

The central topic of this work is to emphasize the different kinds of behavior in the electrical conductivity due to resonances when NNN interactions are included, as happens in carbon nanotubes [24]. Usually, the NNN interaction is not taken into account in graphene tight-binding calculations [25], so here we propose a systematic study of the subject. This study is important because there is a debate concerning which mechanisms determine the charge carrier mobility [26,27], as well as the nature of the minimal conductivity [3]. As we will see, an impurity can produce a sharp peak or a smoothing effect in the electrical conductivity, depending on the charge doping, temperature, strength of the impurity scattering and the value of the NNN interaction. The interplay between such factors is subtle since, for example, the Fermi level and the resonance energy are not shifted by the same amount when the NNN interaction is included. It is worthwhile mentioning that the electrical conductivity at high temperatures is determined basically by the electron–phonon interaction [28], while here we discuss only scattering by impurities. Thus, our results are relevant for basically low temperatures. However, this case is important to explain the weak temperature dependence of the conductivity, which is proportional to the carrier concentration [4,29].

The layout of this work is the following. In Section 2, we describe the model and the perturbative approach used to calculate the Green's function for a NNN tight-binding Hamiltonian of doped graphene. Section 3 describes the calculation of Green's function of pure graphene, which is used in Section 4 to calculate the resonant energies. Section 5 contains the electrical conductivity calculations using the Kubo–Greenwood formula. Finally, in Section 6 we present the conclusions.

2. Model

As a model, we consider a pure graphene tight-binding Hamiltonian with substitutional impurities at very low concentrations. Since there are no correlations between impurities and the impurity concentration is very low, we can reduce the problem to a single localized impurity in a graphene lattice. The behavior for a given low concentration can be found by a simple implementation of the virtual crystal approximation (VCA) [30]. Also, we will use the fact that the graphene's honeycomb lattice is formed by two triangular interpenetrating sublattices, denoted A and B [22]. The corresponding tight-binding Hamiltonian is

$$\mathcal{H} = \mathcal{H}_0 + \mathcal{H}_1 \tag{1}$$

$$\mathcal{H}_0 = -t \sum_{\langle i|j\rangle, \sigma} \left(a^\dagger_{\sigma,i} b_{\sigma,j} + b^\dagger_{\sigma,j} a_{\sigma,i} \right)$$
$$- t' \sum_{\langle\langle i|j\rangle\rangle, \sigma} \left(a^\dagger_{\sigma,i} a_{\sigma,j} + b^\dagger_{\sigma,i} b_{\sigma,j} + a^\dagger_{\sigma,j} a_{\sigma,i} + b^\dagger_{\sigma,j} b_{\sigma,i} \right) \tag{2}$$

$$\mathcal{H}_1 = \varepsilon \left(a^\dagger_{\sigma,l} a_{\sigma,l} \right) \quad \text{or} \quad \mathcal{H}_1 = \varepsilon \left(b^\dagger_{\sigma,l} b_{\sigma,l} \right), \tag{3}$$

where $a_{\sigma,i}$ ($a^\dagger_{\sigma,i}$) annihilates (creates) an electron with spin σ ($\sigma = \uparrow, \downarrow$) on site i at position $\mathbf{R}_i$ on the A sublattice (an equivalent definition is used for the B sublattice), $t(\approx 2.79\,\text{eV})$ is the NN hopping energy, and $t'(\approx 0.68\,\text{eV})$ is the NNN hopping energy [31]. ε is the energy difference between a carbon atom and a foreign atom, and l is the impurity position.

Usually, the resonances are characterized by looking at the Green's functions (G) of $\mathcal{H}$. Expressing G as a perturbation series in terms of G_0 (which is the Green's function corresponding to the unperturbed Hamiltonian $\mathcal{H}_0$), a closed expression is obtained for the local density of states (LDOS) in the impurity site l [30],

$$\rho(l; E) = \frac{\rho_0(l; E)}{|1 - \varepsilon G_0(l, l; E)|^2}, \tag{4}$$

where $G_0(l, l; E)$ and $\rho_0(l; E)$ are, respectively, the Green's function and the LDOS on site l with $\mathcal{H}_0$.

The term $|1 - \varepsilon G_0(l, l; E)|^2$ cannot become zero for E within the band. However, for certain values of ε, this term is near to zero for a given $E \approx E_r$. Then, a sharp peak in the LDOS will emerge around E_r. This E_r is associated with a resonant state inasmuch as there is a different impurity energy level. If $\text{Im}\{G_0(l, l; E)\}$ is a slowly varying function of E (for E around E_r), then the resonant energy will be given as a solution of the Lifshitz equation,

$$1 - \varepsilon \text{Re}\{G_0(l, l; E)\} \approx 0. \tag{5}$$

Furthermore, if the derivative of $\text{Re}\{G_0(l, l; E)\}$ does not have a strong dependence on E near E_r, then [30],

$$\frac{1}{|1 - \varepsilon G_0(l, l; E)|^2} \sim \frac{\Gamma^2}{(E - E_r)^2 + \Gamma^2}, \tag{6}$$

where Γ corresponds to the width of the impurity resonance,

$$\Gamma = \frac{|\text{Im}\{G_0(l, l; E_r)\}|}{|\text{Re}\{G_0'(l, l; E_r)\}|}. \tag{7}$$

Thus, the resonant state effect is sketched by its location, E_r, in Equation (5), and its width, Γ, in Equation (7). These characteristics of the resonant state are inherited from the behavior of the Green's function, which is presented in the next section.

3. Green's function of pure Graphene with NNN interaction

To solve the Lifshitz Equation (5), we need to obtain the Green's function for graphene with NNN interaction. Notice that analytical expressions are only available for the NN interaction [32], and not for the NNN interaction. The Green's function can be obtained from,

$$G_0(E) = \left[\frac{1}{N} \sum_{\mathbf{k} \in 1BZ} \frac{1}{E + is - E(\mathbf{k})} \right], \tag{8}$$

where $s \ll 1$ and $E(\mathbf{k})$ is the dispersion relationship of Equation (2), and is given by [22],

$$E_{\pm}(\mathbf{k}) = \pm t\sqrt{3 + f(\mathbf{k})} - t'f(\mathbf{k}), \tag{9}$$

$$f(\mathbf{k}) = 2\cos\left(\sqrt{3}k_y a\right) + 4\cos\left(\frac{\sqrt{3}}{2}k_y a\right)\cos\left(\frac{3}{2}k_x a\right), \tag{10}$$

where the minus sign applies to the valence band and the plus sign to the conduction band. Around the Dirac point ($\mathbf{K}$ or $\mathbf{K}'$), the momentum can be written as $\mathbf{k} = \mathbf{K} + \mathbf{q}$, where $\mathbf{q}$ is a small vector. Then, Equation (9) up to second order is given by [22],

$$E_{\pm}(\mathbf{K} + \mathbf{q}) \approx 3t' \pm \frac{3ta}{2}|\mathbf{q}|$$
$$- \left\{ \frac{9t'a^2}{4} \pm \frac{3ta^2}{8}\sin\left[3\left(\arctan\frac{q_x}{q_y}\right)\right] \right\}|\mathbf{q}|^2, \tag{11}$$

where a is the carbon–carbon distance ($a \approx 1.42\,\text{Å}$).

To compute Equation (8), we used a square mesh in the first Brillouin zone of the reciprocal space to evaluate the sum over states. The results are presented in Figure 1. In Figure 1a, we show the result when the NNN behavior is absent ($t' = 0$). For the case of pure NN interaction, the obtained Green's function is in excellent agreement with the analytical formula [32], while for the NNN interaction, our results are similar to those obtained by other groups [18]. Notice how at zero energy (corresponding to the Fermi energy for pure graphene, E_F^0), the imaginary and real parts of the Green's function cross at zero energy, resulting in a symmetrical
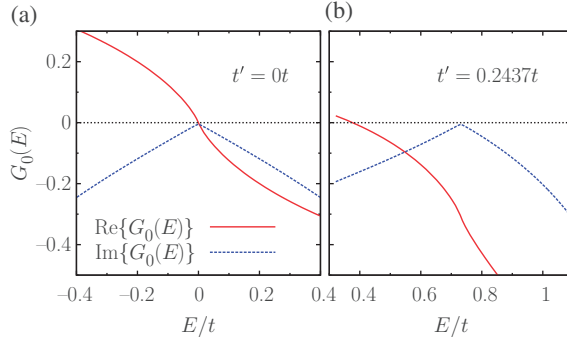
Figure 1. (a) Green's functions with nearest neighbor interaction and (b) with next-nearest neighbor interaction. (The square mesh in the first Brillouin zone that was used to calculate $G_0(l, l; E)$ is uniform and contains $N = 7.5 \times 10^7$ points, and $s = 2 \times 10^{-3}$.)

behavior for ε around $E = 0$, Equation (5). This symmetry is broken when $t' \neq 0$, as seen in Figure 1b. This is due to the fact that the real part of the Green's function no longer crosses the zero at $E_F^0 = 3t'$; this energy value matches with the zero value of the imaginary part.

4. Green's function of a single impurity in graphene

Once the Green's function G_0 for pure graphene is known, we can compute G in order to describe the resonant states. In the following subsections, we present the corresponding results.

4.1. *Local density of states*

The LDOS can be calculated from Equation (4), since

$$\rho_0(l; E) = -\frac{1}{\pi} \text{Im}\big\{G_0(l, l; E)\big\}. \tag{12}$$

Using the calculated G_0, and considering strong impurities, i.e. $\varepsilon/t > 3$, in Figure 2 we can see that the LDOS exhibits a peak at certain resonant energies for two combinations of impurity self-energies ε and different NNN interaction t'. An evident characteristic is that the resonant energy has a shift depending on the t' parameter. This is a consequence of the shift in the ordinate axis of Re $\{G_0(l, l; E)\}$, as observed in Figure 1. Another characteristic that corresponds to the sharpest LDOS behavior emerges when E_r is near E_F^0. From Figure 2, it is clear that the NNN interaction radically changes the resonance properties when compared with the NN case. Therefore, the NN interaction is not enough to describe the behavior of the doped system. To see this, in the following section we calculate the position of the resonant energy and the resonance width.
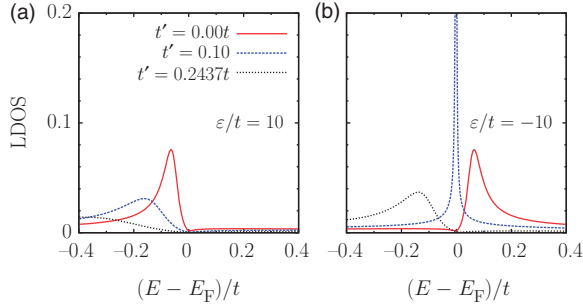
Figure 2. LDOS calculated using Equation (4) for different values of ε and t'. (The parameters used to generate the graphs are the same as those used in Figure 1.)
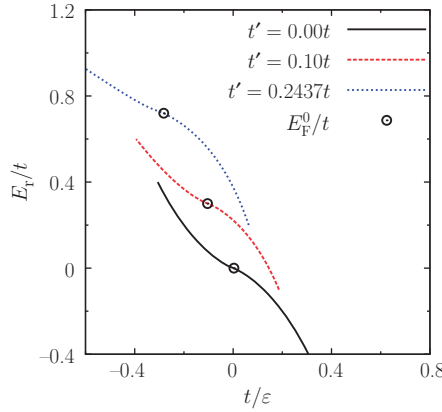

Figure 3. The $E_r = E_r(\varepsilon)$ curve defined by the Lifshitz Equation (5), for different values of the NNN interaction t'. The Fermi energy for pure graphene including NNN interaction, E_F^0, is identified by a circle. (The parameters used to generate the graphs are the same as those used in Figure 1.)

4.2. Resonant energy

In order to obtain E_r, we need to solve the Lifshitz Equation (5). As a result, in Figure 3 we present the energies E_r that satisfy Equation (5) as a function of ε for different sets of t'. The main effect of the NNN interaction is a shift proportional to t', as expected from the first correction to the NN interaction in Equation (11). However, the curvature of $E_r(\varepsilon)$ in Figure 3 exhibits a slight difference as the NNN hopping energy varies. Additionally, in the same figure we plot the Fermi energy E_F^0 for pure graphene including the NNN interaction for a certain ε at which the Fermi energy lies exactly at the resonance LDOS peak. In other words, the circles in Figure 3 are the values of the parameters ε and t' where the electronic properties are most affected, since electrons at the Fermi level have the exact energy of a resonant

state and can thus be easily trapped for a certain amount of time around the impurity.

For the NN interaction, Skrypnyk found that the position of the resonant state near E_F^0 in the asymptotic limit $\varepsilon \to \pm\infty$ is given by [19],

$$\frac{t}{\varepsilon} \propto \frac{E_r}{t} \ln \left| \frac{E_r}{t} \right|. \tag{13}$$

The previous formula is in perfect agreement with our numerical simulations in the same limit for $t' = 0$, as well as with another independent simulation [18]. Thus, this is another successful limiting test case for the software. Using the idea of a rigid translation of the spectrum, we can modify the previous expression to include the NNN interaction as follows,

$$\frac{t}{\varepsilon} \approx \frac{5}{2\sqrt{3}\pi} \left(\frac{E_r - 3t'}{t} \right) \ln \left| \frac{E_r - 3t'}{t} \right|. \tag{14}$$

(Notice that the numerical factor in the above expression was not reported by Skrypnykv and Loktev [19] since their dispersion relation was not normalized.) This modified formula is in excellent agreement with our simulations.

Although the previous expressions follow the form of a rigid translation of the spectrum with t', the more realistic cases are those of small ε, in which the effects of t' are important, since the resonance peak is not shifted by the same amount. As we will see, this is important when one considers the effects on the electronic conductivity.

4.3. *Resonant width*

In Figure 4, we present the influence of the NNN interaction t' on the resonance width Γ as a function of ε^{-1}. The influence of the NNN due to the asymmetry in the curves for $t' \neq 0$ is evident. Observe that the asymmetry leads to a reduced resonance width for $\varepsilon < 0$ when the NNN interaction increases. This means that the peak is sharper and thus the lifetime of the resonance is increased.

On the contrary, the opposite is observed for $\varepsilon > 0$; i.e. the lifetime of the electron near the impurity is decreased by the NNN interaction. In the asymptotic case of pure NN interaction, the observed behavior in our work is consistent with an independent calculation of Γ [33].

As was previously mentioned, the most important peak in the LDOS is located near the Fermi energy. The ε value corresponding to that energy is clearly observed in Figure 4, which is the graph corresponding to Equation (7).

5. DC conductivity

In this section, we evaluate the electrical conductivity (σ_{xx}) taking into account resonant states and the NNN interaction. To do so, we use the Kubo–Greenwood formula expressed as [30],

$$\sigma_{xx} = \frac{e^2 \hbar}{\pi m^2} \frac{N}{\Omega_0} \int_{-\infty}^{\infty} dE \ \mathcal{T}(E) \left(\frac{\partial f}{\partial E} \right) \Big|_{E+\mu}, \tag{15}$$
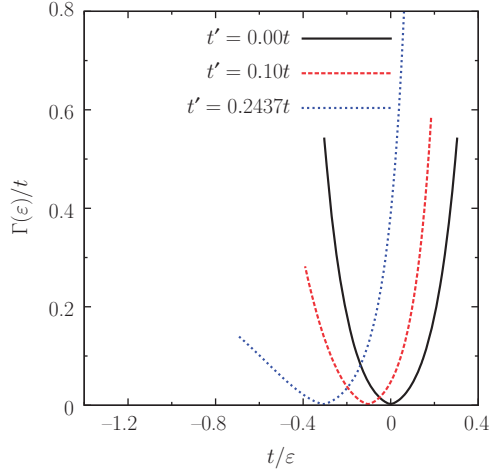
Figure 4. Resonant width, Γ, given by Equation (7) as a function of the impurity self-energy, ε^{-1}. The figure shows asymmetric curves due to the NNN interaction. (The parameters used to generate the graphs are the same as those used in Figure 1.)

where,

$$\mathcal{T}(E) = \mathrm{Tr}\{p_x \mathrm{Im}\{G(E)\} p_x \mathrm{Im}\{G(E)\}\}, \tag{16}$$

and $\Omega_0 = 3a^2$ is the area of the primitive cell, f is the Fermi–Dirac distribution and μ is the chemical potential, which can be tuned by the external field (for example, with a voltage applied in the lattice). p_x is the momentum operator, given by the following commutator,

$$p_x = \frac{im}{\hbar}[\mathcal{H}, x]. \tag{17}$$

It is necessary to remark that here the Hamiltonian operator includes the next-nearest neighbor interaction. Therefore, p_x inherits this interaction and p_x can be written in terms of the momentum operator associated with the NN interaction as follows. Consider first the momentum p_x for NN,

$$p_x^{\mathrm{NN}} = \frac{imt}{\hbar}[x, \mathcal{W}], = \frac{imt}{\hbar} \sum_{l=1}^{N} \sum_{m \in \mathrm{NN}} (\mathbf{R}_l - \mathbf{R}_m)_x \mathcal{W}, \tag{18}$$

where we introduced the connectivity matrix defined as,

$$\mathcal{W}(m, n) = \begin{cases} 1 & \text{if } m \text{ and } n \text{ are NN} \\ 0 & \text{otherwise.} \end{cases} \tag{19}$$

Using this connectivity matrix, the Hamiltonian without perturbation including the NNN interaction can be rewritten as,

$$\mathcal{H}_0 = -t\mathcal{W} - t'(\mathcal{W}^2 - 3\mathcal{I}), \tag{20}$$
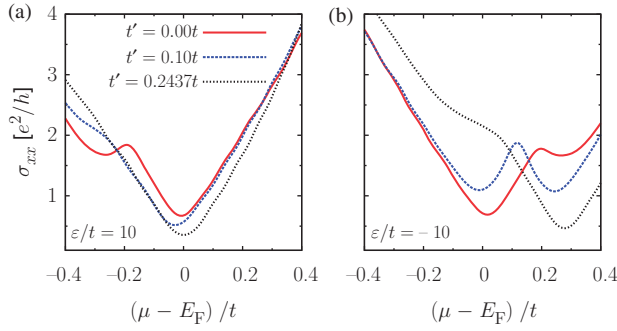
Figure 5. Electrical conductivity calculated using the Kubo–Greenwood formula at low concentration of impurities, $C = 0.01$: (a) $\varepsilon/t = 10$; (b) $\varepsilon/t = -10$. (All lattices have $N \approx 10^4$.)

where $\mathcal{I}$ is the identity matrix. Taking the previous expression and using (18), we obtain the corresponding operator for the NNN case,

$$
\begin{aligned}
p_x^{\mathrm{NNN}} &= \frac{im}{\hbar}[-t\mathcal{W} - t'(\mathcal{W}^2 - 3\mathcal{I}), x], \\
&= p_x^{\mathrm{NN}} + \frac{t'}{t}\left(p_x^{\mathrm{NN}}\mathcal{W} + \mathcal{W}p_x^{\mathrm{NN}}\right).
\end{aligned}
\tag{21}
$$

The previous expressions were written into a computer program, in which we considered a low concentration of impurities, C, introduced by adding the perturbation $\mathcal{H}_1$ at different sites taken at random with a uniform distribution. In Figure 5, we show the conductivity calculated using the Kubo–Greenwood formula (15) for different values of t', and as a function of the charge doping. Figure 5 was computed at a fixed representative temperature, in this case $k_\mathrm{B}T = 0.025\,\mathrm{eV}$, to highlight the main effects of the NNN interaction. Clearly, Figure 5 exhibits the radical difference in the behavior of the conductivity due to the NNN interaction, since a smearing effect, as seen in Figure 5a, can appear, or as in Figure 5b, a sharp peak can be observed. In fact, if we look at the temperature behavior, we can also get very different kinds of behavior of σ_{xx}. These changes are due to a subtle interplay between the chemical doping, temperature, the NNN interaction and the impurity type.

To understand the diverse behavior of σ_{xx}, in Figure 6 we show a sketch of the "building blocks" that appear in the Kubo–Greenwood formula, and how such blocks are modified by the considered parameters. In each panel of the graph, on the left we show the shape of the term $\partial f/\partial E$, which corresponds to the "thermal selector". At $T = 0$, it becomes a delta function centered on the chemical potential (μ), while for $T \neq 0$ it has a width of the order of $k_\mathrm{B}T$. The position of $\partial f/\partial E$ on the energy axis can be externally modified by doping with charge carriers, resulting in different positions of the Fermi energy ($E_\mathrm{F} - \mu$) when compared with the equilibrium value of such energy, denoted by E_F. The second building block is $\mathcal{T}(E)$, which can
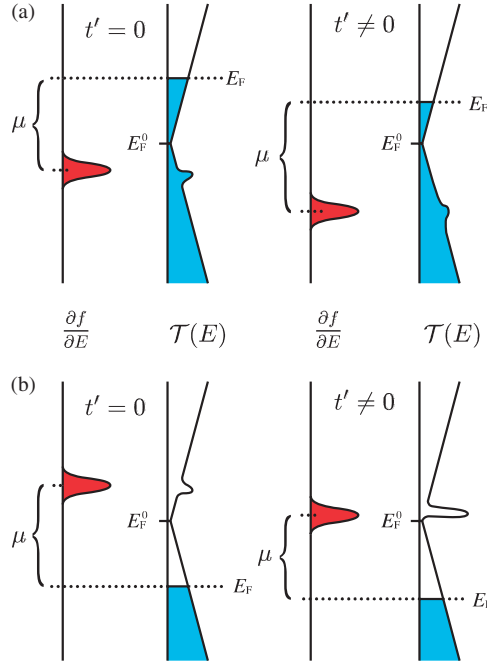
Figure 6. Schematic diagram of the Kubo–Greenwood formula which explains the effect of the NNN interaction. The behavior of the two building blocks, the thermal selector of states $\partial f/\partial E$ and the trace $\mathcal{T}(E)$, are shown on each panel. The position of the resonance energy and Fermi energy are also shown. The following cases are considered: (a) $\varepsilon/t = 10$ and (b) $\varepsilon/t = -10$. Both graphs assume the case $t'/t = 0.1$.

be thought of as a quantum transmittance of the transport channels. Since the Green's function of doped graphene can be written as,

$$G \approx G_0 + \sum_l \frac{G_0 |l\rangle \varepsilon \langle l| G_0}{1 - \varepsilon G_0(l, l)} \tag{22}$$

(where the sum is carried over impurity sites), $\mathcal{T}(E)$ has two types of behavior. Near the resonant energies, G is dominated by the second term in Equation (22), and G_0 can be neglected. As a consequence, a peak appears in the conductivity at the resonant energy, as shown in Figure 6. Far from the resonance, $G \approx G_0$. Then we recover the transmittance of pure graphene.

Now we can study how the two building blocks interact to produce many different kinds of behavior. First, it is clear that variations in μ and T can produce peaks in the conductivity if the thermal selector coincides with the resonance peak. The conductivity can be enhanced if, for example, at a certain temperature the thermal selector begins to have an overlap over the peak of $\mathcal{T}(E)$. The effect of the NNN interaction is very subtle since in principle one can expect a simple translation in energy of the spectrum. However, as stated in the previous sections, the rigid translation of the spectrum is only valid at high ε. According to our results,

for realistic impurities there are deviations from such behavior, and thus E_F and E_r are not rigidly translated, i.e. the distance $|E_F - E_r|$ depends on the NNN interaction. Since the conductivity depends a lot on this factor due to the position of the thermal selector, the resulting effect of the NNN happens to be very important. Also, the resonant peak energy is changed depending on the kind of impurity. As a result of all these factors, we can expect wide variations in the conductivity when disorder is present, as has been observed experimentally in carbon nanotubes [24], and very recently in graphene [34,35]. Furthermore, the present work gives clues about the nature of the minimal conductivity in pristine graphene, since two kinds of mechanism have been proposed to explain the phenomena: the presence of disorder or the tunneling of evanescent waves [3]. Here, we show that the conductivity is very sensitive to disorder and does not produce a universal value for such conductivity, in agreement with the results of Ziegler [36].

Finally, the scattering term in Equation (22) allows us to define a relaxation time, τ_s, measured in seconds, as follows,

$$\frac{1}{\tau_s} = \frac{N_{\text{imp}}}{N} \mathcal{P},$$
(23)

where N_{imp} is the total number of impurities and $\mathcal{P}$ is the total transition rate due to scattering. Notice that $\mathcal{P}$ has units of inverse seconds and is given by summing over all transition rates (the probabilities per unit time) [30],

$$\mathcal{P} = \sum_{\mathcal{I},\mathcal{F}} \varrho_{\mathcal{IF}},$$
(24)

from an initial state $|\mathcal{I}\rangle$ to a final state $|\mathcal{F}\rangle$,

$$\varrho_{\mathcal{IF}} = f_{\mathcal{I}}(1 - f_{\mathcal{F}}) W_{\mathcal{IF}}.$$
(25)

Using the Fermi golden rule,

$$W_{\mathcal{IF}} = \frac{2\pi}{\hbar} |\langle \mathcal{F}|Q|\mathcal{I}\rangle|^2 \delta(E_{\mathcal{F}} - E_{\mathcal{I}}),$$
(26)

where

$$|\langle \mathcal{F}|Q|\mathcal{I}\rangle|^2 = \frac{\varepsilon^2}{|1 - \varepsilon G_0(l, l; E)|^2}$$
$$\approx \frac{1}{\pi^2 \rho_0^2(l; E_r)} \frac{\Gamma^2}{(E - E_r)^2 + \Gamma^2}.$$
(27)

After steps similar to those used to get the Kubo–Greenwood formula [30], we obtain,

$$\mathcal{P} = \frac{\in \pi \|_B \mathcal{T}}{\hbar} \int_{-\infty}^{\infty} d\mathcal{E} \ \mathcal{Q}(\mathcal{E}) \left(\frac{\partial \{}{\partial \mathcal{E}}\right),$$
(28)

where,

$$\mathcal{Q}(E) \approx \frac{\rho^2(E)}{\rho_0^2(l; E_r)} \frac{\Gamma^2}{(E - E_r)^2 + \Gamma^2}. \tag{29}$$

Far from the resonance peak, E_r, and near E_F^0,

$$\rho(E) \approx \frac{1}{\sqrt{3}\pi} \frac{|E - E_F^0|}{t^2}, \tag{30}$$

then the scattering term $\mathcal{Q}(E)$ is given by,

$$\mathcal{Q}(E) \approx \frac{1}{3\pi^2} \frac{1}{\rho_0^2(l; E_r)} \frac{\Gamma^2}{(E_F^0 - E_r)^2 + \Gamma^2} \frac{|E - E_F^0|^2}{t^4}. \tag{31}$$

At $T = 0$, for the resulting relaxation time obtained from a straightforward evaluation of Equation (28) using (31) and remembering that $E_F^0 = 3t'$, we obtain

$$\tau_s^{-1} \approx \frac{4C}{3h} \frac{k_B T}{\rho_0^2(l; E_r)} \frac{\Gamma^2}{(3t' - E_r)^2 + \Gamma^2} \frac{|E_F - 3t'|^2}{t^4}. \tag{32}$$

Thus, the mean free path (ℓ) is $\ell \approx v_F \tau_s$, which goes as E_F^{-2}.

6. Conclusions

We have studied the effects on the spectrum and electronic conductivity of low concentrations of impurities in graphene when the next-nearest neighbor interaction is considered in a tight-binding approximation. Although the electronic spectrum is basically similar to the case of pure nearest neighbor interaction, the conductivity is much more affected since the Fermi level and the resonance peak are not shifted by the same amount, resulting in a wide variability of the conductivity, as happens with carbon nanotubes [24]. As a consequence, the minimal electrical conductivity for graphene with disorder depends on the particular kind of impurity scattering. This assertion has been confirmed very recently by using different kinds of samples [37]. For pristine graphene, our results suggest that the universal value of the minimal conductivity cannot be explained by disorder, in agreement with the ideas of Ziegler [36]. An alternative explanation is the tunneling of evanescent modes through the Dirac point [3,37] . Finally, we obtained the relaxation time in graphene due to impurity scattering, which leads to a large electronic mean free path.

References

[1] K.S. Novoselov, A.K. Geim, S.V. Morozov, D. Jiang, Y. Zhang, S.V. Dubonos, I.V. Grigorieva and A.A. Firsov, Science 306 (2004) p.666.
[2] A.K. Geim, Science 324 (2009) p.1530.
[3] N.M.R. Peres, J. Phys. Condens. Matter 21 (2009) p.323201.
[4] K.S. Novoselov, A.K. Geim, S.V. Morozov, D. Jiang, M.I. Katsnelson, I.V. Grigorieva, S.V. Dubonos and A.A. Firsov, Nature 438 (2005) p.197.
[5] A.A. Balandin, S. Ghosh, W. Bao, I. Calizo, D. Teweldebrhan, F. Miao and C.N. Lau, Nano Lett. 8 (2008) p.902.
[6] P. Avouris, Z. Chen and V. Perebeinos, Nature Nanotechnol. 2 (2007) p.605.
[7] M.I. Katsnelson and K.S. Novoselov, Solid State Commun. 143 (2007) p.3.
[8] P.G. Silvestrov and K.B. Efetov, Phys. Rev. Lett. 98 (2007) p.016802.
[9] J. Bai, X. Zhong, S. Jiang, Y. Huang and X. Duan, Nature Nanotechnol. 5 (2010) p.190.
[10] F.J. López-Rodríguez and G.G. Naumis, Phys. Rev. B 78 (2008) p.201406.
[11] F.J. López-Rodríguez and G.G. Naumis, Phil. Mag. 90 (2010) p.2977.
[12] G.G. Naumis, Phys. Rev. B 76 (2007) p.153403.
[13] A. Bostwick, J.L. McChesney, K.V. Emtsev, T. Seyller, K. Horn, S.D. Kevan and E. Rotenberg, Phys. Rev. Lett. 103 (2009) p.056404.
[14] D. Wei, Y. Liu, Y. Wang, H. Zhang, L. Huang and G. Yu, Nano Lett. 9 (2009) p.1752.
[15] I. Gierz, C. Riedl, U. Starke, C.R. Ast and K. Kern, Nano Lett. 8 (2008) p.4603.
[16] M. Amini, S.A. Jafari and F. Shahbazi, Europhys. Lett. 87 (2009) p.37002.
[17] J. Schleede, G. Schubert and H. Fehske, Europhys. Lett. 90 (2010) p.17002.
[18] V.M. Pereira, J.M.B. Lopes dos Santos and A.H. Castro Neto, Phys. Rev. B 77 (2008) p.115109.
[19] Yu.V. Skrypnyk and V.M. Loktev, Phys. Rev. B 73 (2006) p.241402.
[20] Yu.V. Skrypnyk and V.M. Loktev, Phys. Rev. B 75 (2007) p.245401.
[21] T.O. Wehling, A.V. Balatsky, M.I. Katsnelson, A.I. Lichtenstein, K. Scharnberg and R. Wiesendanger, Phys. Rev. B 75 (2007) p.125425.
[22] A.H. Castro Neto, F. Guinea, N.M.R. Peres, K.S. Novoselov and A.K. Geim, Rev. Mod. Phys. 81 (2009) p.109.
[23] V.M. Pereira, F. Guinea, J.M.B. Lopes dos Santos, N.M.R. Peres and A.H. Castro Neto, Phys. Rev. Lett. 96 (2006) p.036801.
[24] Z. Zhang, D.A. Dikin, R.S. Ruoff and V. Chandrasekhar, Europhys. Lett. 68 (2004) p.713.
[25] A. Lherbier, X. Blase, Y.-M. Niquet, F. Triozon and S. Roche, Phys. Rev. Lett. 101 (2008) p.036808.
[26] T.O. Wehling, S. Yuan, A.I. Lichtenstein, A.K. Geim and M.I. Katsnelson, Phys. Rev. Lett. 105 (2010) p.056802.
[27] A. Cresti, N. Nemec, B. Biel, G. Niebler, F. Triozon, G. Cuniberti and S. Roche, Nano Res. 1 (2008) p.361.
[28] S. Yuan, H. De Raedt and M.I. Katsnelson, Phys. Rev. B 82 (2010) p.115448.
[29] Z.H. Ni, L.A. Ponomarenko, R.R. Nair, R. Yang, S. Anissimova, I.V. Grigorieva, F. Schedin, P. Blake, Z.X. Shen, E.H. Hill, K.S. Novoselov and A.K. Geim, Nano Lett. 10 (2010) p.3868.
[30] E.N. Economou, *Green's Functions in Quantum Physics*, 3rd ed., Springer Series in Solid-State Sciences, Springer-Verlag, Heidelberg, 2006.
[31] A. Grüneis, C. Attaccalite, L. Wirtz, H. Shiozawa, R. Saito, T. Pichler and A. Rubio, Phys. Rev. B 78 (2008) p.205425.
[32] T. Horiguchi, J. Math. Phys. 13 (1972) p.1411.
[33] T.O. Wehling, M.I. Katsnelson and A.I. Lichtenstein, Chem. Phys. Lett. 476 (2009) p.125.

[34] S. Jung, G.M. Rutter, N.N. Klimov, D.B. Newell, I. Calizo, A.R. Hight-Walker, N.B. Zhitenev and J.A. Stroscio, Nature Phys. 7 (2011) p.245.
[35] V.W. Brar, R. Decker, H.M. Solowan, Y. Wang, L. Maserati, K.T. Chan, H. Lee, Ç.O. Girit, A. Zettl, S.G. Louie, M.L. Cohen and M.F. Crommie, Nature Phys. 7 (2010) p.43.
[36] K. Ziegler, Phys. Rev. B 75 (2007) p.233407.
[37] Y. Sui, T. Low, M. Lundstrom and J. Appenzeller, Nano Lett. 11 (2011) p.1319.